Hydroxyl-bearing bortolanite from the Lovozero alkaline massif, Kola Peninsula

Ekaterina A. Selivanova[*,1,2], Yakov A. Pakhomovsky[1,2], Lyudmila M. Lyalina[1], Alena A. Kompanchenko[1], Julia A. Mikhailova[1,2], Andrey A. Zolotarev (jr)[3]

[1] Geological Institute, Kola Science Centre of the Russian Academy of Sciences, 14 Fersman Street Apatity 184209 Murmansk Region Russia

[2] Nanomaterials Research Centre, Kola Science Centre of the Russian Academy of Sciences, 14 Fersman Street Apatity 184209 Murmansk Region Russia

[3] St. Petersburg State University, Department of Crystallography, 7/9 Universitetskaya Emb. St. Petersburg 199034 Russia

Abstract

Bortolanite, a rare mineral of the rinkite group, seidozerite supergroup occurs in two different associations in the Lovozero massif (Kola Peninsula, Russia): (1) together with ferri-katophorite and phlogopite, it forms porous or mesh aggregates (symplektitic accretions) with euhedral contours in the contact zone of a volcano-sedimentary xenolith and eudialyte lujavrite, Kuamdespakhk Mt and (2) in intergrowths with titanite and fluorcaphite in the poikilitic feldspathoid syenites, Sengischorr Mt. In both cases, bortolanite was found in association with rosenbushite that is close to it in chemical composition, but unlike bortolanite, it contains no

[*] e.selivanova@ksc.ru
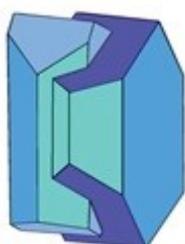
*REE*s. The mineral is triclinic, space group $P\text{-}1$, $a = 9.5807(5)$, $b = 5.6943(4)$, $c = 7.2813(4)$ Å, $\alpha = 89.891(5)°$, $\beta = 100.959(4)°$, $\gamma = 101.241(5)°$, $V = 382.25(4)$ Å^3, $Z = 1$.

The Lovozero bortolanite differs from the Brazilian holotype sample (type locality TL) due to the presence of (OH)-groups in its composition, which is indicated by Raman′s data. A combination of single-crystal X-ray diffraction data and electron microprobe data provides the following crystal-chemical formula:

$(Ca_{1.97}Ce_{0.01}Nd_{0.01}Th_{0.01})_{\Sigma 2} (Ca_{1.39}Zr_{0.61})_{\Sigma 2} (Na_{0.72}Ca_{0.28})_{\Sigma 1}(Na_{1.36}Ca_{0.56}Mn_{0.03}Zn_{0.01})_{\Sigma 1.96}$ $(Ti_{0.78}Zr_{0.08}Nb_{0.05}Mg_{0.05}Fe_{0.04})_{\Sigma 1} Si_4O_{14}((OH)_{0.92}O_{0.87}F_{0.21})_{\Sigma 2} F_2.$
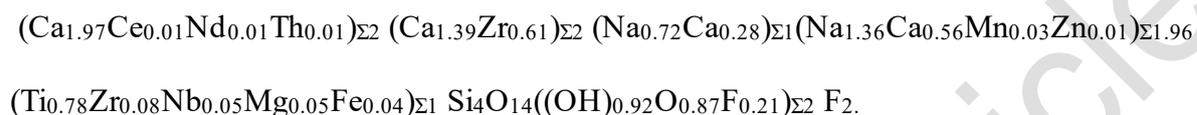
Key words: bortolanite, titanosilicate, rinkite group, alkaline rocks, crystal structure, Lovozero, Kola Peninsula, Arctic

Introduction

The list of mineral species in one of the richest mineralogical provinces of the world, the Lovozero alkaline massif, contains more than 400 species, of which about a third are rare and the rarest ones. The rinkite group (Table 1), which is belongs to the seidozerite supergroup (Sokolova and Cámara, 2017), includes 14 mineral species and is currently represented in the Lovozero massif by the following four species (marked in bold in Table 1): rinkite-(Ce) $(Ca_3REE)Na(NaCa)Ti(Si_2O_7)_2(OF)F_2$, rosenbuschite $Ca_6Zr_2Na_6ZrTi(Si_2O_7)_4(OF)_2F_4$, seidozerite $Na_2Zr_2Na_2MnTi(Si_2O_7)_2O_2F_2$ and bortolanite $Ca_2(Ca_{1.5}Zr_{0.5})Na(NaCa)Ti(Si_2O_7)_2(OF)F_2$ described in this study. Two more minerals, mosandrite-(Ce) (referred as "hydro-rincolite") and götzenite, were mentioned, but not reliably characterized (Semenov, 1972). In recent decades, much attention has been paid to the minerals of this group: classification principles have been developed (Sokolova and Cámara, 2017), the nomenclature has been revised; and new mineral species such as batievaite-(Y) (Lyalina et al., 2016), rinkite-(Y) (Pautov et al., 2019) and nacareniobsite-(Y) have been discovered (Agakhanov et al., 2023).

Thus, bortolanite (Btln), $Ca_2(Ca_{1.5}Zr_{0.5})Na(NaCa)Ti(Si_2O_7)_2(OF)F_2$, was discovered in nepheline syenites of the Poços de Caldas alkaline massif, Minas Gerais, Brazil. The mineral was

named after the Bortolan quarry. The IMA Commission on New Minerals, Nomenclature and Classification (CNMNC) approved it in 2021 under the number IMA2021-040a, and in 2022 a complete study of the mineral was published (Day et al., 2022).

The authors of this study have found bortolanite in two locations in the Lovozero massif: (1) at the contact of alkaline rocks with roof xenoliths (Kuamdespakhk Mt) and (2) in poikilitic feldspathoid syenites (Sengischorr Mt). This article is devoted to the characterization and discussion of the specific properties of the Lovozero bortolanite, which is the second find of this mineral in the world and the first one in Russia. At the same time, this article is not a simple description of a specific case, but expands knowledge about mineralogical relationships, as well as crystal chemistry and isomorphism of rinkite-related minerals in general.

Table 1. Ideal structural formulae for rinkite group minerals.

Mineral	Sites of ideal structural formula					
	$2A^P$ $2M^H$	$4M^O$			$2X^O_M$	$2X^O_A$
Mosandrite-(Ce)	Ca_2 $(CaREE)$	$(H_2O)_2$	Ti	$(Si_2O_7)_2$	$(OH)_2$	$(H_2O)_2$
Rinkite-(Ce)	Ca_2 $(CaREE)$	$Na(NaCa)$	Ti	$(Si_2O_7)_2$	(OF)	F_2
Nacareniobsite-(Ce)	(Ca_3REE)	Na_3	Nb	$(Si_2O_7)_2$	(OF)	F_2
Seidozerite	Na_2 Zr_2	Na_2Mn	Ti	$(Si_2O_7)_2$	O_2	F_2
Grenmarite	Na_2 Zr_2	Na_2Mn	Zr	$(Si_2O_7)_2$	O_2	F_2
Rosenbuschite	Ca_4 Ca_2Zr_2	Na_2Na_4	TiZr	$(Si_2O_7)_4$	O_2F_2	F_4
Kochite	Ca_2 $MnZr$	Na_3	Ti	$(Si_2O_7)_2$	OF	F_2
Götzenite	Ca_2 Ca_2	$NaCa_2$	Ti	$(Si_2O_7)_2$	(OF)	F_2
Hainite-(Y)	Ca_2 (CaY)	$Na(NaCa)$	Ti	$(Si_2O_7)_2$	(OF)	F_2
Fogoite-(Y)	Ca_2 Y_2	Na_3	Ti	$(Si_2O_7)_2$	(OF)	F_2
Batievaite-(Y)	Ca_2 Y_2	$\square(H_2O)_2$	Ti	$(Si_2O_7)_2$	$(OH)_2$	$(H_2O)_2$
Rinkite-(Y)	Ca_2 (CaY)	$Na(NaCa)$	Ti	$(Si_2O_7)_2$	(OF)	F_2
Nacareniobsite-(Y)	Ca_2 (CaY)	Na_3	Nb	$(Si_2O_7)_2$	(OF)	F_2
Bortolanite	$Ca_{3.5}Zr_{0.5}$	$Na(NaCa)$	Ti	$(Si_2O_7)_2$	OF	F_2
Bortolanite from Lovozero	$Ca_{3.5}Zr_{0.5}$	$Na(NaCa)$	Ti	$(Si_2O_7)_2$	**O(OH)**	F_2

Data given according to (Sokolova and Cámara, 2017), except for rinkite-(Y) (Pautov et al., 2019), nacareniobsite-(Y) (Agakhanov et al., 2023) and bortolanite (Day et al., 2022). The mineral species known in the Lovozero massif in bold.

Sites given according to (Sokolova, 2006): M^H = cations of the H sheet; M^O = cations of the O sheet; A^P = cations at the peripheral (P) sites, $2X^O_M + 2X^O_A$ = anions of the O sheet not shared with Si_2O_7 groups.

Geological background

The Lovozero alkaline massif (Fig. 1a), which formed 360–370 Ma (Kramm and Kogarko, 1994; Wu et al., 2010; Mitchell et al., 2011), is a layered laccolith located in the southwest of the Kola Peninsula (Russia) among Archean gneisses and granite-gneisses.

The Lovozero massif consists of the following three main units (Fig. 1a): Layered, Eudialyte and Poikilitic complexes (Vlasov et al., 1959; Gerasimovsky et al., 1966; Bussen and Sakharov, 1972). The first, Layered, complex consists of numerous sub-horizontal layers (or rhythms). Each of the rhythms is a sequence of the following rocks: lujavrite – foyaite – urtite or lujavrite – foyaite. Lujavrite is a trachytoid meso- to melanocratic nepheline syenite; foyaite is a massive to weakly trachytoid leucocratic nepheline syenite; urtite is a massive monomineral nepheline rock. The main rock type of the Eudialyte complex is lujavrite enriched in eudialyte-group minerals, so-called eudialyte lujavrite. The third, Poikilitic, complex comprises of leucocratic feldspathoid (nepheline, sodalite or vishnevite) syenites. A distinctive feature of these rocks is the poikilitic texture when feldspar laths contain numerous inclusions of feldspathoids. Rocks of the Poikilitic complex form lenses, or irregularly shaped bodies, which are located in both the Layered and Eudialyte complexes.

A large number of roof xenoliths of Devonian volcaniclastic rocks, both unaltered and intensely metasomatized, are found among the rocks of the Layered and Eudialyte complexes (Gerasimovsky et al., 1966; Korchak et al., 2011). The unaltered xenoliths are composed of olivine basalt, basalt tuff, tuffite and sandstone. Under the influence of solutions sourced from alkaline magma, these rocks were metasomatically altered towards an alkali-syenitic composition.

The Lovozero massif is widely known for its unique mineral diversity as it represents a type locality for 110 minerals; in total, there are 412 valid mineral species there (https://www.mindat.org/loc-2697.html, Page updated: March 10, 2024). The maximal mineral diversity, including rare and endemic species, is typical of pegmatites and hydrothermal veins (Semenov, 1972; Pekov, 2001). However, as studies of recent years show, new and rare minerals can also be found in alkaline rocks: these are zolotarevite, sapozhnikovite and a number of minerals of the cancrinite group, e.g., kyanoxalite, hydroxycancrinite, cancrisilite and others.

Analytical methods

For this study, two samples of rocks from the Lovozero massif were selected. Sampling points are shown in Figure 1a. Sample LV-152/4 was collected at the contact of xenolith of volcanoclastic rock and eudialyte lujavrite (Fig. 1b), and sample LV-02-1-3 is a fragment of poikilitic feldspathoid syenite (Fig. 1d).

The mineral associations, their relationships and chemical composition were studied using LEO-1450 SEM equipped with an AZtec ULTIM MAX 100 OXFORD instruments.

The mineral composition was also determined by an electron microprobe at the Geological Institute, Kola Science Centre, Apatity, using a Cameca MS-46 microprobe at an accelerating voltage of 22 kV and a probe current of 30–40 nA. Quantitative point analyses were made with a defocused (10–15 μm) beam. The following standards were used: wollastonite (Si Kα, Ca Kα), hematite (Fe Kα), lorenzenite (Na Kα, Ti Kα), pyrope (Mg Kα, Al Kα), $MnCO_3$ (Mn Kα), metallic Nb Lα, $ZrSiO_4$ (Zr Lα), $SrSO_4$ (Sr Lα), (La,Ce)S (La Lα), CeS (Ce Lα), $LiNd(MoO_4)_2$ (Nd Lα), wadeite (K Kα), sphalerite (Zn Kα) and thorite (Th Lα). The fluorine (Kα) content was measured by EDS of AZtec ULTIM MAX 100 using as standard the fluorapatite pre-analysed by WDS of Cameca MS-46.
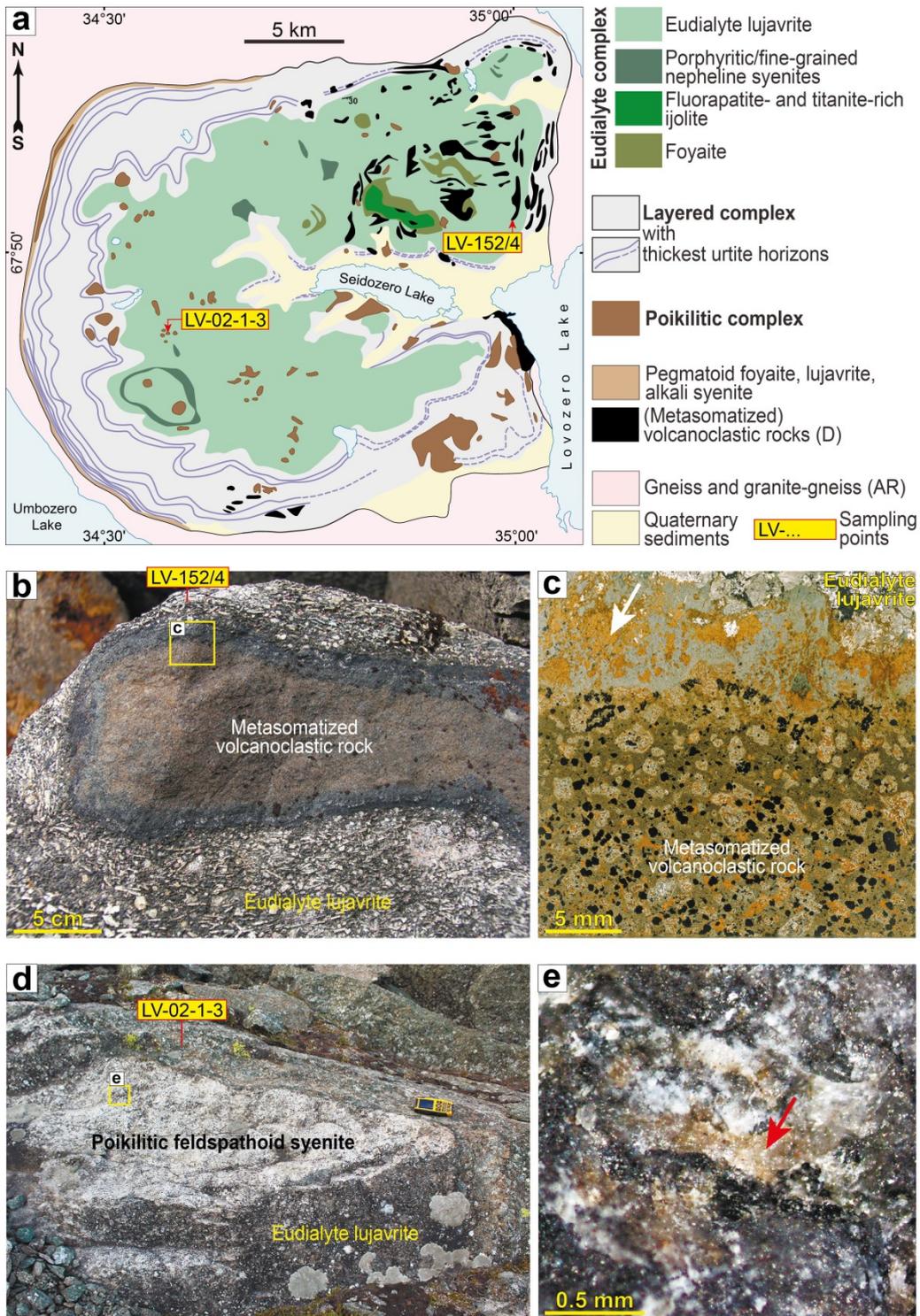
Fig. 1. Geological scheme of the Lovozero alkaline massif after (Saprykina et al., 1977), with simplifications (a) and sampling points. (b) xenolith of volcanoclastic rock in eudialyte lujavrite (sampling point LV-152/4); (c) photo of a thin section of LV-152/4 in transmitted light; the white arrow shows the bortolanite location; (d) poikilitic feldspathoid syenite in eudialyte lujavrite (sampling point LV-02-1-3); (e) photo of sample LV-02-1-3; the red arrow shows the bortolanite location.

For a single-crystal study, a fragment of a bortolanite crystal with a size of 0.17 × 0.13 × 0.08 mm was cut from a segment of the thin section LV-152/4 shown in Figure 2b. A single-crystal X-ray diffraction study of this fragment was performed using a Rigaku XtaLAB Synergy-S diffractometer (MoKα radiation, 293K) with a microfocus X-ray source PhotonJet-S and a high-speed hybrid photon counting detector HyPix-6000HE at the X-Ray diffraction Centre of St. Petersburg State University. The CrysAlisPro software was used for data processing (CRYSALISPRO, 2015). The absorption correction was introduced using the SCALE3 ABSPACK algorithm. The structures have been solved and refined using the ShelX program package (Sheldrick, 2015) within the Olex2 shell (Dolomanov et al., 2009). The crystal data and structure refinement details are given in Table 3; atom coordinates and displacement parameters are in Tables 4 and 5. The selected interatomic distances and bond-valence values are shown in Table 6 and Table 7 respectively. Site occupancy and refined site-scattering data are shown in Table 8. Upon the completion of this study, a polished sample was prepared from the above fragment and its chemical composition was determined (an. 1252 and 1253 in Table 2).

The Raman spectra of minerals were obtained using EnSpectr R532 and R785 spectrometers (Spectr-M, ISSP RAS, Chernogolovka, Russia) equipped with an Olympus BX-43 microscope at the Mining Institute KSC RAS. Raman spectra were excited using a 532 nm solid-state laser with an actual power of 18 mW and a 785 nm diode laser with an actual power of 150 mW under the 50× objective (NA 0.75). The spectra were obtained in the range of 160–4000 cm^{-1} at a resolution of 4–6 cm^{-1} to the 532 nm laser and in the range of 160-2850 cm^{-1} at a resolution of 7-9 cm^{-1} to the 785 nm laser at room temperature. To improve the signal-to-noise ratio, the number of acquisitions was set to 30. All spectra were processed using the algorithms implemented in the OriginPro 8.1 software package (Originlab Corporation, Northampton, MA, USA).

Bortolanite morphology and associations

The sample LV-152/4 mainly consists of phlogopite and ferri-katophorite. Accessory minerals are nepheline, natrolite, fluorapatite and pyrrhotite. Other minerals of the association are as follows: potassic-arfvedsonite, richterite, thomsonite-Ca, loparite-(Ce), titanite, perovskite, ilmenite, sphalerite, magnetite, pyrite, chalcopyrite, violarite, bartonite, rosenbuschite, mosandrite-(Ce), rhabdophane-(Ce), fluorite, etc.

Bortolanite is represented by two types of aggregates. The first type is represented by aggregates of a reticulated (sometimes closer to a layered one due to phlogopite plates) structure without definite boundaries in the mass of hornfels (Fig. 2a); the size of aggregates reaches approximately 2.5 mm. In the centre, most continuous even sections of the aggregates, bortolanite has a pronounced block structure with a block size of 20-50 μm in combination with noticeable compositional heterogeneity (Fig. 2b). At the boundary with the amphibole-phlogopite mass there are areas with an increased content of *REE*s, up to mosandrite-(Ce), in back-scattered electron images (BSE images) these areas have a lighter shade (Fig. 2a). Areas with a mesh structure often contain clusters of rosenbushite grains with a size of about 5-20 μm, which is very close to bortolanite in chemical composition, but with clear boundaries. Some clusters have an increased content of Nb, in this case they have a lighter shade in BSE and become clearly visible against the background of bortolanite (Fig. 2c).

The second type includes symplektitic accretions of bortolanite–phlogopite–ferri-katophorite with clear idiomorphic contours of the primary mineral replaced by them. This variety of bortolanite (Fig. 2d,e) occurs, unlike the first one, somewhat removed from the contact of rocks.

In the sample LV-02-1-3 bortolanite also occurs in association with potassic feldspar, nepheline, sodalite, natrolite, aegirine, aegirine-augite, loparite-(Ce), titanite, fluorcaphite, phlogopite, ferri-katophorite, rosenbuschite, fluorapatite, pyrrhotite, mosandrite-(Ce), ilmenite, sphalerite, magnetite, hematite, tausonite, pyrophanite, zircon, vishnevite, pyrochlore group minerals, etc. The mineral is often located in the feldspar matrix (Fig. 3a); sometimes it also
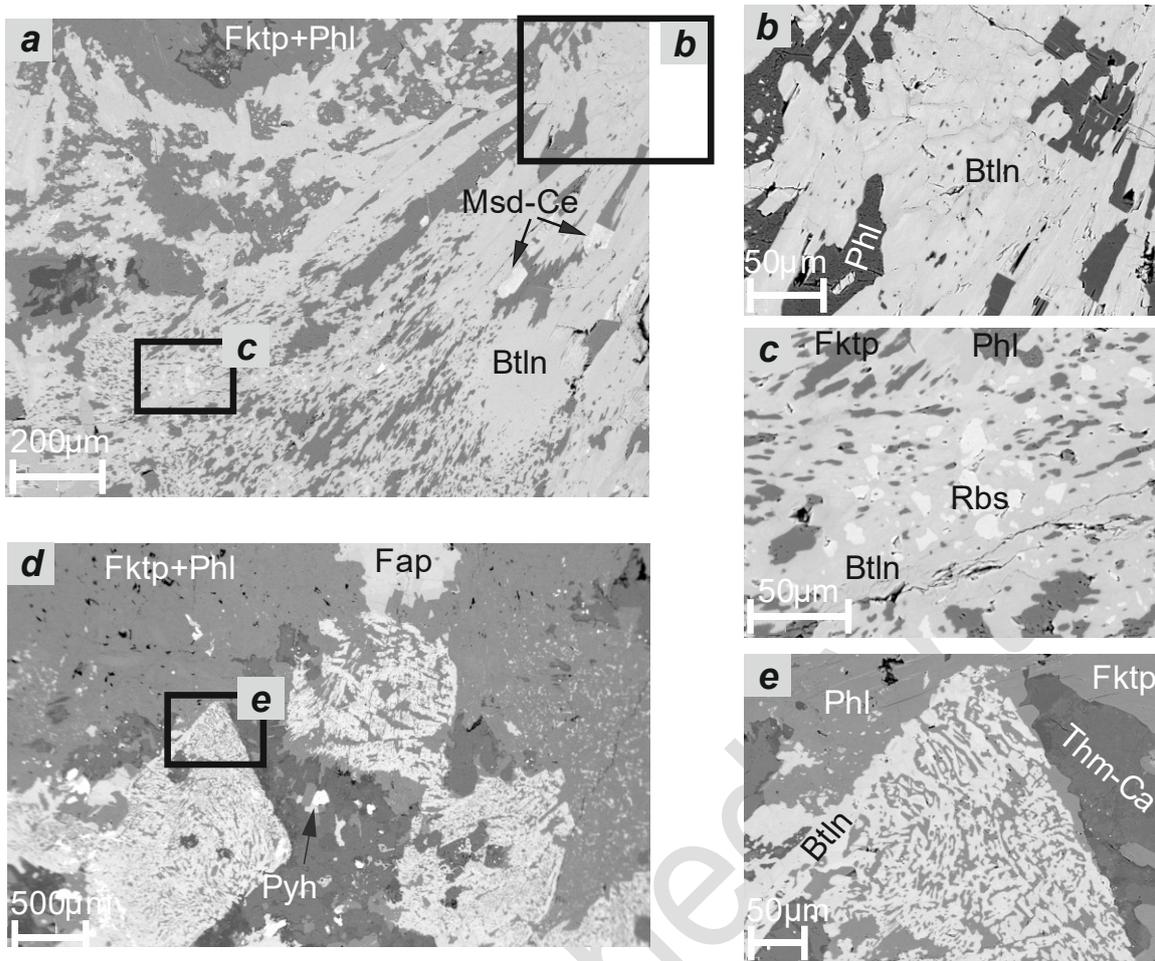
Fig. 2. Morphology of bortolanite from the contact zone of volcanoclastic xenolith with eudialyte lujavrite, Kuamdespakhk Mt, Lovozero massif, sample LV-152/4; BSE image; (a) aggregates with a mesh structure, (b,c) detailed BSE image of Figure 2a. (d) – symplektitic accretions of the bortolanite–phlogopite–ferri-katophorite with euhedral contours; (e) detailed BSE image of Figure 2d;

Btln – bortolanite, Phl – phlogopite, Fktp – ferri-katophorite, Rbs – rosenbuschite, Fap – fluorapatite, Pyh – pyrrhotite, Msd-Ce – mosandrite-(Ce), Thm-Ca – thomsonite-Ca

comes into contact with nepheline or is surrounded by a nepheline rim. Figure 3c shows a wide nepheline border impregnated with aegirine. Phase heterogeneity is manifested in the largest grains, up to 1 mm in size, with an irregular shape and uneven boundaries (see BSE images in Fig. 3a,c). The lighter and more homogeneous (pristine-looking with smooth surface) areas correspond to the bortolanite, while the darker altered patches are characterized by a deficit of

total sum obtained by electron microprobe analysis (EMPA), greater heterogeneity, and the spots of high Nb content (Fig. 3b).
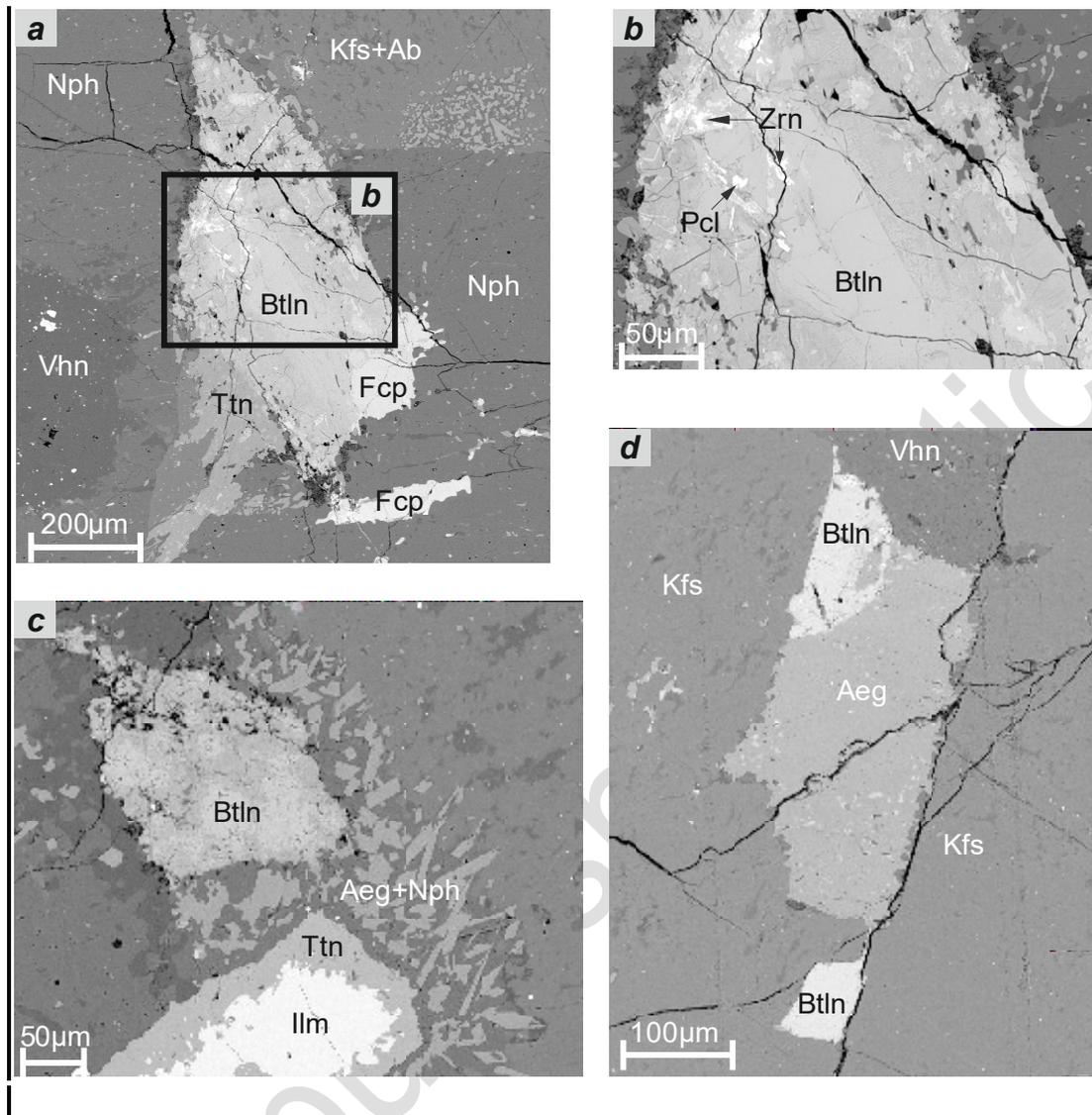
Fig. 3. Morphology of bortolanite from the poikilitic feldspathoid syenites, Sengischorr Mt, Lovozero massif, sample LV-02-1-3; BSE image: (a) bortolanite intergrowths with titanite and fluorcaphite; (b) detailed BSE image of Figure 3a; (c) aegirine-nepheline crowns around the bortolanite; (d) well-shaped bortolanite grains in potassic feldspar in intergrowths with aegirine; Btln – bortolanite, Kfs – potassic feldspar, Nph – nepheline, Aeg – aegirine, Ttn – titanite, Fcp – fluorcaphite, Vhn – vishnevite, Zrn – zircon, Pcl – pyrochlore group minerals, Ilm – ilmenite

Sometimes these grains intergrow with titanite and fluorcaphite (Fig. 3a). Bortolanite from the syenites typically contains zircon inclusions (Fig. 3b); inclusions of the pyrochlore group

minerals are also occasionally found. Another form of bortolanite is represented in the poikilitic feldspathoid syenites by 10-20 μm inclusions in aegirine or aegirine-augite. There are also inclusions of titanite, rosenbuschite and zircon along with bortolanite. The size of such inclusions sometimes reaches 100 μm and these are well-formed grains (Fig. 3c). It is interesting that rosenbuschite is also present in the poikilitic feldspathoid syenites, and in greater abundance than bortolanite. Unlike the xenoliths, however, these rocks consistently exhibit spatial separation of the two very similar mineral species.

Bortolanite chemical composition

The composition of the Lovozero bortolanite from both types of rocks is close to that of the Brazilian one (Table 2), but differs in a slightly lower *REE* and F content. The slight differences in the content of minor elements are obviously related to the geochemical environment. Thus, the Brazilian bortolanite contains Y and Hf as impurities whereas the Lovozero bortolanite from the contact zone of xenoliths includes Mg, Zn and Th and that from the feldspathoid syenites – K and Sr.

The total sum of the EMPA of Lovozero bortolanite from both types of rocks, as well as the sum for Brazilian bortolanite, has some drawback, but in our case this deficiency is greater. The authors of bortolanite (Day et al., 2022) did not measure water directly, and ignored it in the calculations, having explained this by the crystal chemistry of the rinkite group: *«Sokolova (Sokolova, 2006) pointed out that in Group I [later renamed the rinkite group by Sokolova and Cámara (2017)], the monovalent anion at the X^O_A and X^O_M sites is invariably F^-, as there is insufficient space to accommodate OH and its corresponding hydrogen bond. This conclusion is valid for structures in which all cation sites are fully occupied. However, OH and H_2O groups can occur at the X^O_A and X^O_M sites in a structure where cation sites are partly occupied; cf. batievaite-(Y), a rinkite-group mineral (Lyalina et al., 2016; Table 1). In bortolanite, all cation sites are fully occupied, hence there is no possibility for OH and H_2O groups to occur at the X^O_A*

and X^O_M site». As a result, in the empirical formula of Brazilian bortolanite based on O+F=18 the Si *apfu* is 4.07 that is 1.75% higher than full occupancy - 4.0 *apfu*.

In our study, we were also unable to measure water due to the scarce amount of available material, but the presence of water was confirmed by the Raman's data.

The empirical formula calculated on the basis of 4 (Si+Al) *apfu*, taking into account the requirements for the charge balance and full occupancy of anionic positions, is as follows: $Ca_{4.20}Na_{2.075}Ti_{0.775}Zr_{0.69}Th_{0.005}Nb_{0.045}Mg_{0.045}Fe_{0.035}Mn_{0.03}REE_{0.02}Zn_{0.01}Si_{4.00}O_{14.87}F_{2.21}(OH)_{0.92}$ for samples with a refined crystal structure, average of an. 1252 and 1253 (Table 2).

We also recalculated the data for bortolanite from the TL in the same way (Table 2, last column). The new total sum is closer to 100% , which suggests that this method of calculation is better suited in this case, at least until there is evidence of the complete absence of water in the Brazilian mineral.

In both types of geological environments, the contact zone of xenoliths and feldspathoid syenite of Lovozero massif, bortolanite is associated with rosenbushite, sometimes contacting with the latter in aggregates (Fig. 2c). These minerals are very similar in chemistry (Table 1), but their grains in aggregates are separated by clear phase boundaries. We have included the rosenbushite composition in Table 2 to show very small differences between these two mineral species. The expected quantitative differences can be described by the scheme resulting from the formulas of their end members: $3Ca + Ti \rightarrow 2Zr + 2Na$. That's what we observe in reality (Fig. 4). An interesting qualitative difference lies in the constant presence of *REE*s in bortolanite unlike to their complete absence in rosenbuschite.

Table 2. Chemical composition and unit formula of bortolanite and rosenbuschite from the Lovozero massive (Kola Peninsula, Russia) and bortolanite from *type locality* (TL) (Day et al., 2022).

Sample	poikilitic feldspathoid syenite LV-02/1-3				contact zone of xenoliths LV-152/4					TL
	bortolanite		rosenbuschite		bortolanite				rosenbuschite	bortolanite
No.	**1128**	**1255**	**1256**	**1127**	**1172**	**1173**	**1252**	**1253**	**1171**	
Nb_2O_5	0.88	1.12	0.99	0.82	1.00	0.79	0.78	0.97	n.d.	1.07
SiO_2	30.71	30.96	30.95	31.15	32.12	31.67	31.65	32.63	31.09	32.49
TiO_2	8.68	7.26	6.03	8.07	9.81	8.28	8.17	8.40	6.04	9.94
ZrO_2	10.58	13.53	21.24	14.05	6.98	10.44	11.30	11.31	19.59	6.70
HfO_2	n.d.	n.d.	n.d.	n.d.	n.d.	n.d.	n.d.	n.d.	n.d.	0.20
ThO_2	n.d.	n.d.	n.d.	n.d.	n.d.	n.d.	0.16	0.23	n.d.	n.d.
Al_2O_3	n.d.	0.14	0.08	n.d.	n.d.	n.d.	n.d.	n.d.	n.d.	n.d.
Y_2O_3	n.d.	n.d.	n.d.	n.d.	n.d.	n.d.	n.d.	n.d.	n.d.	0.31
La_2O_3	0.15	n.d.	n.d.	n.d.	0.30	n.d.	n.d.	n.d.	n.d.	0.65
Ce_2O_3	0.50	0.34	n.d.	0.20	0.55	0.26	0.17	0.15	n.d.	1.25
Nd_2O_3	0.25	n.d.	n.d.	n.d.	0.29	0.22	0.23	0.14	n.d.	0.37
Gd_2O_3	n.d.	n.d.	n.d.	n.d.	n.d.	n.d.	n.d.	n.d.	n.d.	0.12
MgO	n.d.	n.d.	n.d.	0.36	n.d.	0.19	0.19	0.25	0.45	n.d.
CaO	30.08	28.44	26.32	29.51	33.03	31.28	31.20	31.64	25.83	31.15
MnO	0.58	0.53	0.41	n.d.	0.25	0.25	0.25	0.25	0.18	1.46
FeO	0.29	0.23	0.37	0.35	0.13	0.31	0.31	0.38	0.37	0.59
ZnO	n.d.	n.d.	n.d.	n.d.	n.d.	n.d.	0.14	0.16	n.d.	n.d.
SrO	1.58	1.93	0.85	0.38	n.d.	n.d.	n.d.	n.d.	n.d.	n.d.
Na_2O	8.06	8.68	8.98	8.17	7.99	8.27	8.43	8.75	9.53	8.36
K_2O	n.d.	0.09	0.05	n.d.	n.d.	n.d.	n.d.	n.d.	n.d.	n.d.
F	4.70	4.70	5.10	5.66	5.69	5.79	5.47	5.76	4.68	6.95
$-O=F_2$	1.98	1.98	2.15	2.38	2.40	2.44	2.30	2.43	1.97	2.93
$H_2O^+_{calc}$*	0.86	1.22	0.23	0.41	1.35	1.15	1.04	1.17	1.23	0.78
Total	**95.92**	**97.19**	**99.45**	**96.75**	**97.09**	**96.46**	**97.19**	**99.76**	**97.02**	**99.46**

|				apfu on the basis Si+Al=4						
Nb	0.05	0.07	0.06	0.05	0.06	0.05	0.04	0.05	n.d.	0.06
Si	4.00	3.98	3.99	4.00	4.00	4.00	4.00	4.00	4.00	4.00
Ti	0.85	0.70	0.58	0.78	0.92	0.79	0.78	0.77	0.58	0.92
Zr	0.67	0.85	1.33	0.88	0.42	0.64	0.70	0.68	1.23	0.40
Hf	n.d.	n.d.	n.d.	n.d.	n.d.	n.d.	n.d.	n.d.	n.d.	0.01
Th	n.d.	n.d.	n.d.	n.d.	n.d.	n.d.	n.d.	0.01	n.d.	n.d.
Al	n.d.	0.02	0.01	n.d.	n.d.	n.d.	n.d.	n.d.	n.d.	n.d.
Y	n.d.	n.d.	n.d.	n.d.	n.d.	n.d.	n.d.	n.d.	n.d.	0.02
La	0.01	n.d.	n.d.	n.d.	0.01	n.d.	n.d.	n.d.	n.d.	0.03
Ce	0.02	0.02	n.d.	0.01	0.03	0.01	0.01	0.01	n.d.	0.06
Nd	0.01	n.d.	n.d.	n.d.	0.01	0.01	0.01	0.01	n.d.	0.02
Mg	n.d.	n.d.	n.d.	0.07	n.d.	0.04	0.04	0.05	0.09	n.d.
Ca	4.20	3.92	3.63	4.06	4.41	4.23	4.23	4.16	3.56	4.11
Mn	0.06	0.06	0.04	n.d.	0.03	0.03	0.03	0.03	0.02	0.15
Fe^{2+}	0.03	0.02	0.04	0.04	0.01	0.03	0.03	0.04	0.04	0.06
Zn	n.d.	n.d.	n.d.	n.d.	n.d.	n.d.	0.01	0.01	n.d.	n.d.
Sr	0.12	0.14	0.06	0.03	n.d.	n.d.	n.d.	n.d.	n.d.	n.d.
Na	2.04	2.16	2.24	2.03	1.93	2.03	2.07	2.08	2.38	2.00
K	n.d.	0.01	0.01	n.d.	n.d.	n.d.	n.d.	n.d.	n.d.	n.d.
H	0.75	1.05	0.20	0.35	1.12	0.97	0.88	0.96	1.06	0.64
F	1.94	1.91	2.08	2.30	2.24	2.31	2.19	2.23	1.90	2.71
O	16.06	16.09	15.92	15.70	15.76	15.69	15.81	15.77	16.10	15.29

[*] The water content in the form of (OH)-groups is calculated from the charge balance and for the full occupancy of anionic positions
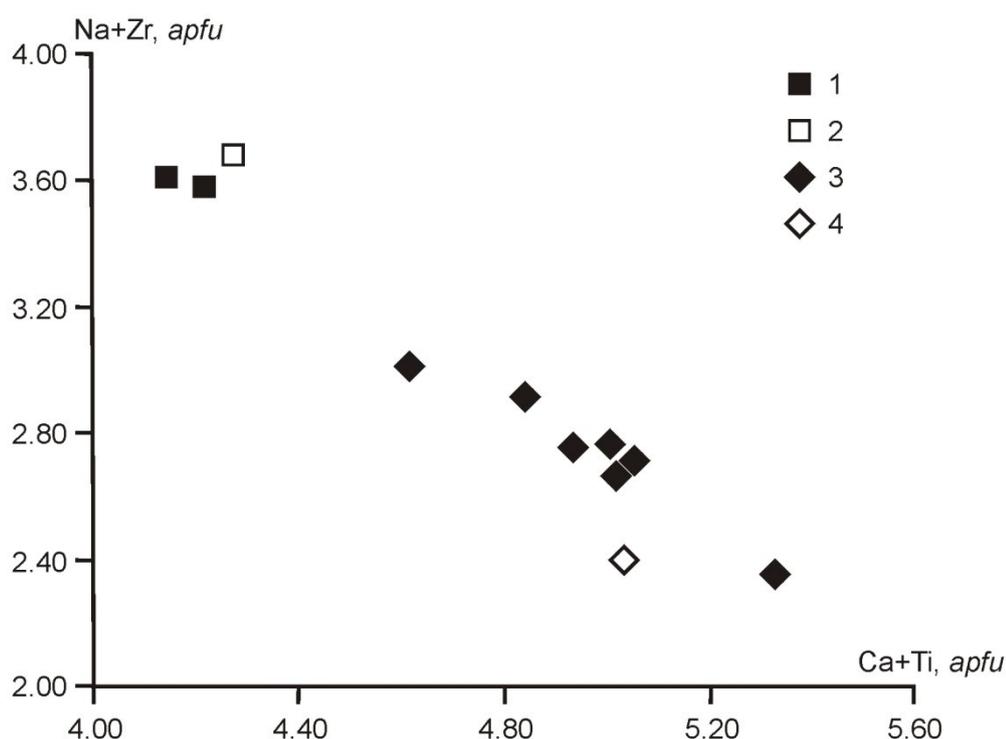
Fig. 4. Concentration of Na+Zr *versus* that of Ca+Ti showing the compositional range of the specimens investigated. 1 – rosenbuschite, Lovozero massif, our data; 2 – rosenbuschite, Lovozero massif (Semenov, 1972); 3 – bortolanite, Lovozero massif, our data; 4 – bortolanite, type locality (Day et al., 2022).

Raman spectroscopy

The spectra of bortolanite from the Lovozero massif, sample LV-152/4 (Fig. 5a) show some common features with the spectra of minerals close to it in chemical composition: götzenite from the same rinkite group (Sharygin et al., 1996, Lafuente et al., 2015) and wöhlerite (Lafuente et al., 2015) from the wöhlerite group (Fig. 5b,c). In the bortolanite Raman spectra, the most intense band at 750-910 cm^{-1} is attributed to symmetric stretching of apical Si-O bonds and symmetric vibrations of the Si-O-Si bridge. The weaker group of bands at 910-1100 cm^{-1} is associated with other internal tetrahedral modes and band at 1058 cm^{-1} corresponds to the
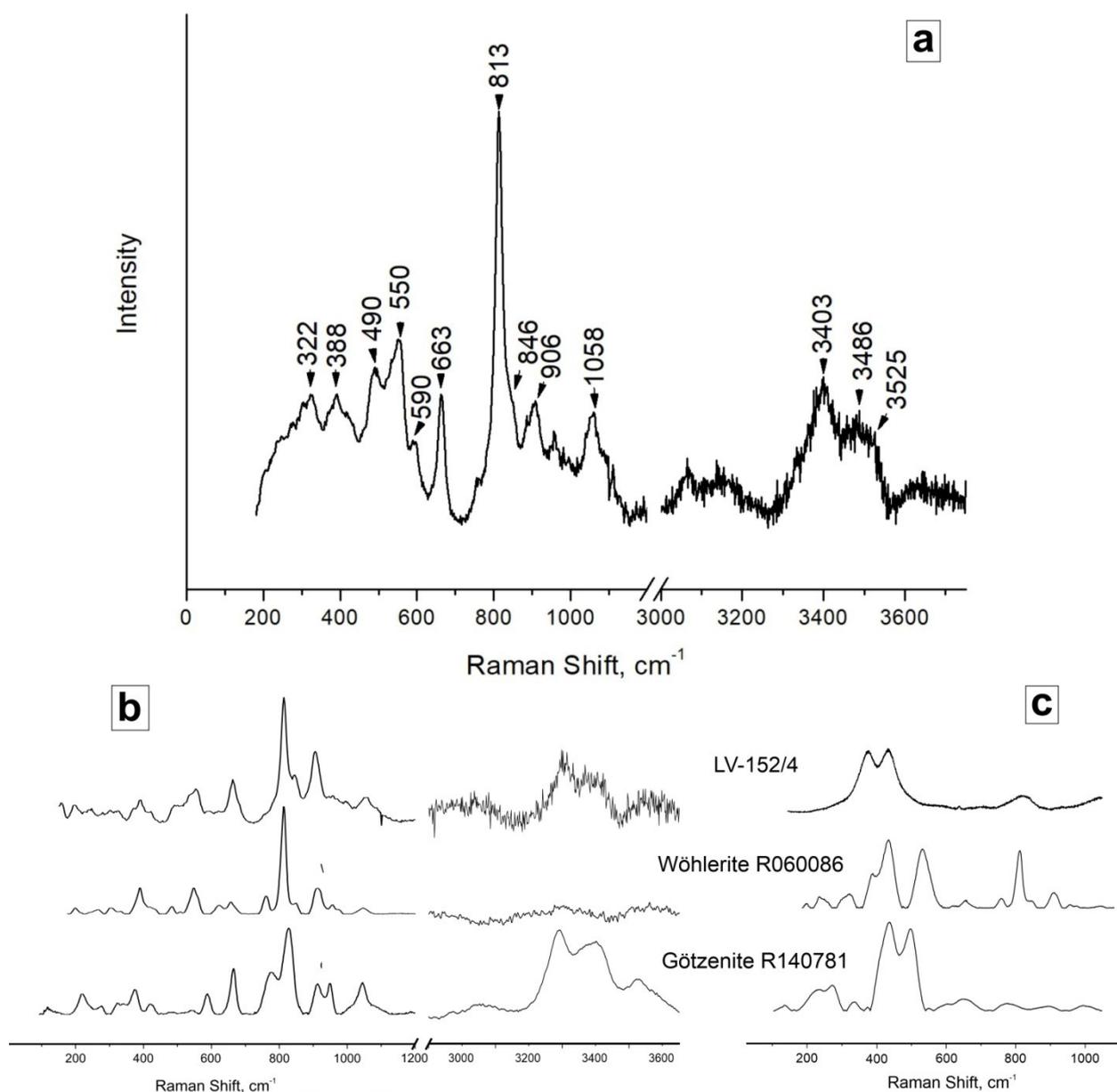
Fig. 5. (a) Raman spectrum of bortolanite with 532 nm laser excitation; (b) its comparison with wöhlerite and götzenite (Lafuente et al., 2015) with 532 nm laser excitation and (c) 780/785 nm laser excitation.

antisymmetric mode of the Si-O-Si bridge. The intense bands at 600-700 cm^{-1} and 400-600 cm^{-1} are mixed. The range at 600-700 cm^{-1} correspond to bending vibrations in Si_2O_7 and Ti(Nb)-O stretching vibrations and probably chemical bonds vibrations formed by the O, F and OH anions. The range at 400-600 cm^{-1} most likely correspond to bending vibrations in Si-O-Si and stretching vibrations in Zr-O. A group of bands in the low-frequency region of 200-400 cm^{-1} is assigned to libration and translation of the Si_2O_7 dimers as well as stretching vibrations of Na-O and Ca-O.

In the 3300–3600 cm^{-1} range, there was a broad band centered at 3403 cm^{-1} with two shoulders at 3486 and 3525 cm^{-1}. According to the literature data, bands between 3000 and 3700 cm^{-1} in minerals correspond to the O-H bonds stretching (Larkin, 2011; Frezzotti et al., 2012; Chukanov and Vigasina, 2020). On the Raman spectra of lamprophyllite group minerals belonging to the seidozerite supergroup like bortolanite, it was shown that in the region 3400–3800 cm^{-1} the OH group and H$_2$O stretching vibrations are present (Andrade et al., 2018; Aksenov et al., 2021).

In the 785 nm laser excitation Raman spectrum three broad bands of 376 cm^{-1}, 432 cm^{-1} and 825 cm^{-1} were observed (Fig. 5c).

The stretching frequency v of the O-H bond obtained by Raman spectroscopy may be used to bond strength evaluation (Emsley, 1980; Libowitzky, 1999). Molecules of H$_2$O exhibit rather long H bonds and high frequencies, whereas OH-groups are distributed from very strong to very weak H bonds and from very low to very high stretching frequencies. Very strong H bonds are observed at frequencies below 1600 cm^{-1} and at d(O···O) < 2.50 Å, strong H bonds are characterized by frequencies between 1600 and 3200 cm^{-1} and O···O distances between 2.50 and 2.70 Å, and weak H bonds occur above 3200 cm^{-1} (up to ~ 3700 cm^{-1}) and at d(O···O) > 2.70 Å (with a barely defined upper limit beyond 3 Å) (Emsley, 1980). In bortolanite from the Lovozero massif, the distances X^O_M···O6 = 2.785 Å, X^O_M···O7 = 2.793 Å, X^O_M···O7 = 2.873 Å, X^O_M···O6 = 2.879 Å (<3 Å, see also Figure in Supplementary materials) and modes in the spectral region 3400-3600 cm^{-1} are in a quite good agreement with those obtained from the distance-frequency correlation (Libowitzky, 1999) and indicates the presence of weak H bonds in the mineral. Minor differences between these values may be due to a significant deviation of the O···H-O angle from 180 degrees.

Crystal structure

The mineral investigated by us in this study is a variety of the recently discovered bortolanite (Day et al., 2022), which belongs to the rinkite group of the seidozerite supergroup (Sokolova

and Cámara, 2017). The crystal structure of this supergroup minerals consists of so-called HOH blocks (or sheets) that is typical of heterophyllosilicates (Ferraris and Gula, 2005; Ferraris, 2008) or, in other words, of minerals with TS (Titanium-Silicate) blocks (Sokolova, 2006; Sokolova and Cámara, 2013).

The H (heteropolyhedral) layer is formed by M^H and A^P polyhedra linked to Si_2O_7 groups. The M^HO_6 and A^PO_6 polyhedra share edges to form double chains parallel to the c axis and linked by the Si_2O_7 groups (Fig. 6a). In case of bortolanite there is a significant amount of Zr in the M^H site. The M^H site is an octahedron occupied by Ca and Zr with the 0.70:0.30 ratio, respectively (Table 8). The average $< M^H\text{-}\varphi >$ bond length is 2.289 Å (φ = O, F, OH). The A^P site has CN equal to 7 and is almost fully occupied by Ca (with a small amount of REEs). The average $< A^P\text{-}\varphi >$ bond length is 2.478 Å.
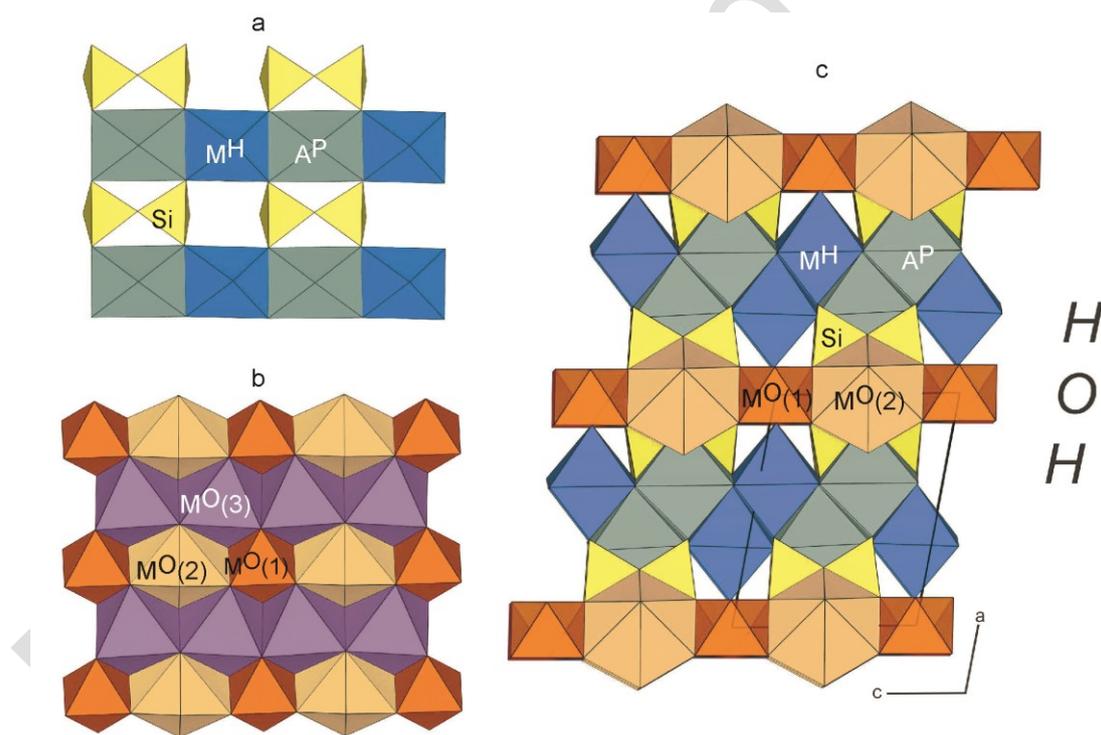
Fig. 6. The crystal structure of the Lovozero bortolanite: (a) the H layer: M^H and A^P polyhedra linked with Si_2O_7 groups; (b) the O layer: two columns extending along the c axis: one column of M^O3 octahedra, the second of alternating polyhedra M^O2 and M^O1; (c) general view of the crystal structure, projection along the axis b.

The *O* (octahedral) layer is formed by polyhedra centered by the M^O3, M^O2 and M^O1 cations. This layer can be considered as consisting of two columns that extend along the *c* axis (Fig. 6b).

One column is formed by the M^O3O_6 octahedra and the other is composed of alternating M^O2 and M^O1 polyhedra. The M^O3 octahedra are occupied by Na and Ca with a 0.68:0.28 ratio respectively (and a small amount of Mn and Zn). The average $< M^O3 - \varphi>$ bond length is 2.366 Å. The M^O2 position (CN 8) is occupied by Na0.72Ca0.28 (see Table 8) with an average $< M^O2-\varphi >$ bond length of 2.470 Å. Ti (with a small amount of Zr, Nb, Mg and Fe) are concentrated in the M^O1 site with an average $< M^O1 - \varphi >$ bond length of 2.001 Å. In contrast to the holotype sample of bortolanite (Day et al., 2022), in our case there is practically no distortion of this octahedral M^O1 position (Table 6).

Table 3. Crystal data and structure refinement of the Lovozero bortolanite

Crystal system	triclinic
Space group	*P*-1
a, Å	9.5807(5)
b, Å	5.6943(4)
c, Å	7.2813(4)
α, °	89.891(5)
β, °	100.959(4)
γ, °	101.241(5)
Volume, Å^3	382.25(4)
Z	1
ρ_{calc},g/cm^3	3.275
μ, mm^{-1}	3.149
F(000)	368.0
Crystal size, mm^3	0.17 × 0.13 × 0.08
Radiation	Mo Kα (λ = 0.71073)
Temperature, K	293(2)
2Θ range for data collection, °	6.504 to 59.99
Index ranges	-13 ≤ h ≤ 13, -8 ≤ k ≤ 8, -10 ≤ l ≤ 10
Reflections collected	6008
Independent reflections	2198 [R_{int} = 0.0381, R_{sigma} = 0.0523]
Independent reflections with I>=2σ (I)	1650
Data/restraints/parameters	2198/0/145
Goodness-of-fit on F^2	1.076
Final R indexes [I>=2σ (I)]	R_1 = 0.0510, wR_2 = 0.1324
Final R indexes [all data]	R_1 = 0.0673, wR_2 = 0.1452
Largest diff. peak/hole / e Å^{-3}	1.80/-0.87

Table 4. Atomic coordinates and equivalent isotropic displacement parameters (Å^2) of the Lovozero bortolanite

Atom	x	y	z	U(eq)
M^H	0.64043(6)	0.21591(11)	0.91081(8)	0.0113(2)
M^O3	0.99473(11)	0.49734(19)	0.24513(14)	0.0175(5)
A^P	0.63706(8)	0.21885(15)	0.40961(11)	0.0144(3)
M^O2	0	0	½	0.0188(8)
M^O1	0	0	0	0.0167(4)
Si1	0.71409(11)	0.7423(2)	0.65579(16)	0.0112(3)
Si2	0.71794(12)	0.7430(2)	0.20724(17)	0.0131(3)
O1	0.7437(4)	0.7728(10)	0.4387(5)	0.0505(13)
O2	0.6140(3)	0.9341(6)	0.6714(5)	0.0203(7)
O3	0.6127(4)	0.9233(6)	0.1353(5)	0.0254(8)
O4	0.6416(4)	0.4694(6)	0.6724(5)	0.0255(8)
O5	0.6585(4)	0.4664(6)	0.1529(5)	0.0258(8)
O6	0.8765(3)	0.8114(6)	0.7764(5)	0.0261(8)
O7	0.8806(3)	0.8274(6)	0.1740(5)	0.0254(8)
X^O_M	0.8810(3)	0.2568(6)	0.9660(4)	0.0206(10)
X^O_A	0.8834(3)	0.2978(5)	0.4746(4)	0.0231(6)

Table 5. Anisotropic displacement parameters (Å^2) of the Lovozero bortolanite

Atom	U_{11}	U_{22}	U_{33}	U_{23}	U_{13}	U_{12}
M^H	0.0150(3)	0.0099(3)	0.0080(3)	0.0000(2)	0.0029(2)	-0.0007(2)
M^O3	0.0281(8)	0.0141(8)	0.0132(7)	0.0017(5)	0.0056(5)	0.0099(5)
A^P	0.0148(5)	0.0161(5)	0.0109(4)	-0.0004(3)	0.0031(3)	-0.0013(3)
M^O2	0.0165(11)	0.0157(12)	0.0230(12)	-0.0007(8)	0.0031(7)	0.0012(7)
M^O1	0.0163(5)	0.0209(6)	0.0083(5)	-0.0018(4)	0.0032(3)	-0.0083(4)
Si1	0.0097(5)	0.0079(6)	0.0159(6)	-0.0001(4)	0.0003(4)	0.0032(4)
Si2	0.0119(5)	0.0099(6)	0.0185(6)	0.0013(4)	0.0026(4)	0.0051(4)
O1	0.043(2)	0.095(4)	0.0119(17)	0.001(2)	0.0079(16)	0.008(2)
O2	0.0181(15)	0.0133(16)	0.0323(18)	0.0023(14)	0.0079(13)	0.0071(12)
O3	0.0280(17)	0.0206(18)	0.0305(18)	0.0000(15)	0.0001(14)	0.0171(14)
O4	0.0296(18)	0.0092(16)	0.037(2)	-0.0028(14)	0.0103(15)	-0.0027(13)
O5	0.0344(19)	0.0113(16)	0.0318(19)	0.0006(14)	0.0099(15)	0.0012(14)
O6	0.0190(15)	0.0233(19)	0.0327(19)	-0.0063(15)	-0.0064(13)	0.0071(13)
O7	0.0181(15)	0.0219(19)	0.039(2)	0.0053(16)	0.0099(14)	0.0068(13)
X^O_M	0.0184(15)	0.0277(19)	0.0162(15)	-0.0006(12)	0.0004(10)	0.0088(12)
X^O_A	0.0173(12)	0.0267(16)	0.0259(14)	-0.0010(12)	0.0023(10)	0.0078(11)

Table 6. Selected bond lengths of the Lovozero bortolanite (Å).

Atom	Atom	Length	Atom	Atom	Length	Atom	Atom	Length
M^H	$O2^1$	2.316(3)	M^O3	$O6^7$	2.358(4)	Si1	O1	1.661(4)
	$O3^4$	2.346(4)		O7	2.362(3)		O2	1.605(3)
	$O3^2$	2.359(4)		$X^O_M{}^7$	2.404(3)		O4	1.588(3)
	O4	2.256(4)		$X^O_M{}^8$	2.405(3)		O6	1.609(3)
	$O5^3$	2.229(4)		X^O_A	2.327(3)	<Si1 - O>		1.616
	X^O_M	2.229(3)		$X^O_A{}^7$	2.337(3)			
$< M^H - \varphi>$		2.289	$< M^O3 - \varphi >$		2.366	Si2	O1	1.661(4)
							O3	1.595(3)
A^P	$O1^1$	2.910(5)	M^O2	$O1^2$	2.500(4)		O5	1.590(4)
	$O2^2$	2.353(3)		$O1^9$	2.500(4)		O7	1.603(3)
	$O2^1$	2.514(3)		$O6^2$	2.647(4)	<Si2 - O>		1.612
	$O3^1$	2.561(4)		$O6^9$	2.647(4)			
	O4	2.378(4)		$O7^9$	2.539(4)	M^O1	$O6^{12}$	1.996(3)
	O5	2.355(4)		$O7^2$	2.539(4)		$O6^2$	1.996(3)
	X^O_A	2.272(3)		$X^O_A{}^{10}$	2.194(3)		$O7^9$	1.997(3)
$< A^P - \varphi >$		2.478		$X^O_A{}^{11}$	2.194(3)		$O7^{13}$	1.997(3)
			$< M^O2 - \varphi >$		2.470		$X^O_M{}^{10}$	2.010(3)
							$X^O_M{}^{14}$	2.010(3)
						$< M^O1 - \varphi >$		2.001

φ = O, F, OH.
[1] +X,-1+Y,+Z; [2] 1-X,1-Y,1-Z; [3] +X,+Y,1+Z; [4] X,-1+Y,1+Z; [5] 1+X,+Y,+Z; [6] 1+X,1+Y,+Z; [7] 2-X,1-Y,1-Z; [8] +X,+Y,-1+Z; [9] -1+X,-1+Y,+Z; [10] 1-X,-Y,1-Z; [11] -1+X,+Y,+Z; [12] -1+X,-1+Y,-1+Z; [13] 1-X,1-Y,-Z; [14] -1+X,+Y,-1+Z

Table 7. Bond-valence values* for Lovozero bortolanite

| Atom*	Si1	Si2	M^H	A^P	M^O3	M^O2	M^O1	Σ
O1	0.91	0.91		0.09		$0.18^{x2}\downarrow$		2.09
O2	1.05		0.37	0.33				1.98
				0.23				
O3		1.08	0.33	0.20				1.95
			0.34					
O4	1.10		0.43	0.32				1.85
O5		1.09	0.46	0.34				1.89
O6	1.03				0.27	$0.12^{x2}\downarrow$	$0.63^{x2}\downarrow$	2.05
O7		1.06			0.27	$0.16^{x2}\downarrow$	$0.62^{x2}\downarrow$	2.11
X^O_M			0.41		0.21		$0.57^{x2}\downarrow$	1.40
					0.21			
X^O_A				0.32	0.22	$0.29^{x2}\downarrow$		1.04
					0.21			
Total	4.09	4.14	2.34	1.83	1.39	1.50	3.64	

* bond-valence values calculated on the basis our crystallographic information file (CIF) using the ECoN21 program (Ilinca, 2022).

Table 8. Site occupancy and site-scattering for the Lovozero bortolanite

	Site occupancy (according to structure refinement)	Refined site-scattering (epfu)	Calculated site-scattering (epfu)	Site occupancy (taking into account the chemical data, apfu)
M^H	$Ca_{0.653(5)}Zr_{0.347(5)}$	53.88	52.20	$Ca_{1.39}Zr_{0.61}$
A^P	$Ca_{0.983(2)}Ce_{0.017(2)}$	41.30	41.48	$Ca_{1.97}Ce_{0.01}Nd_{0.01}Th_{0.01}$
M^O3	$Na_{0.501(14)}Ca_{0.499(14)}$	30.98	27.22	$Na_{1.36}Ca_{0.56}Mn_{0.03}Zn_{0.01}$
M^O2	$Na_{0.669(18)}Ca_{0.331(18)}$	13.98	13.52	$Na_{0.72}Ca_{0.28}$
M^O1	$Ti_{0.852(8)}Nb_{0.148(8)}$	24.81	24.05	$Ti_{0.78}Zr_{0.08}Nb_{0.05}Mg_{0.05}Fe_{0.04}$
X^O_M	$O_{0.52(6)}F_{0.48(6)}$	16.96	16.22	$(OH)_{0.92}O_{0.87}F_{0.21}$
X^O_A	F	18	18	F_2

The anisotropic displacement parameters of the M^O1 site is lightly elongated along the X^O_M-M^O1-X^O_M bond direction, and it is possible to split this site (with approximate coordinates of additional site -0.012162, 0.025506, -0.003373), but the «main» peak will still remain at the center of the inversion (0, 0, 0). The splitting site will be at a distance of approximately 0.20 Å from it. Thus we do not observe complete displacement of the M^O1 site as reported by (Day et al., 2022). Differences in the character of disordering may still be related to the occupancy of the M^O1 and X^O_M sites itself, which is different in the two samples. The X^O_M site is mixed O-OH-F anion position with the 0.435:0.46:0.105 ratio, respectively (The scheme of the local environment of X^O_M site in Supplementary materials). One more additional anion position X^O_A is fully occupied by F.

A combination of single-crystal X-ray diffraction and electron microprobe data provides the following empirical formula:

$$^{A^P}_{\square}(Ca^{\square}_{1.97}Ce_{0.01}Nd_{0.01}Th_{0.01})_{\Sigma 2}\ ^{M^H}_{\square}(Ca_{1.39}Zr_{0.61})_{\Sigma 2}\ ^{M^O_1}_{\square}(Ti_{0.78}Zr_{0.08}Nb_{0.05}Mg_{0.05}Fe_{0.04})_{\Sigma 1}$$

$$^{M^O_2}_{\square}(Na_{0.72}Ca_{0.28})_{\Sigma 1}\ ^{M^O_3}_{\square}(Na_{1.36}Ca_{0.56}Mn_{0.03}Zn_{0.01})_{\Sigma 1.96}(Si_2O_7)_2\ ^{X^O_M}_{\square}((OH)_{0.92}O_{0.87}F_{0.21})_{\Sigma 2}\ ^{X^O_A}_{\square}F_2$$
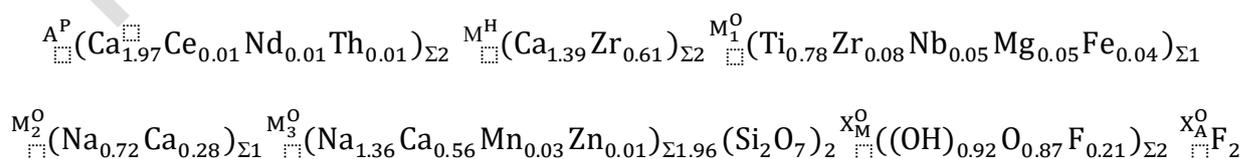
Discussion

Bortolanite, a rinkite group mineral, was discovered in 2022 at the Bortolan Quarry in the Poços de Caldas alkaline massif (Minas Gerais, Brazil). This mineral was found in the nepheline syenite in close intergrowths with götzenite and in association with nepheline, alkali feldspar, aegirine, natrolite, analcime and manganoan pectolite (Day et al, 2022). The simplified formula based on 18 (O + F) *apfu* is as follows: $Ca_2(Ca,Zr)_2Na(Na,Ca)_2Ti(Si_2O_7)_2(O,F)_2F_2$. The crystal-chemical formula of the bortolanite from the Lovozero massif is as follows:

$(Ca_{1.97}Ce_{0.01}Nd_{0.01}Th_{0.01})_{\Sigma 2}$ $(Ca_{1.39}Zr_{0.61})_{\Sigma 2}$ $(Na_{0.72}Ca_{0.28})_{\Sigma 1}(Na_{1.36}Ca_{0.56}Mn_{0.03}Zn_{0.01})_{\Sigma 1.96}$ $(Ti_{0.78}Zr_{0.08}Nb_{0.05}Mg_{0.05}Fe_{0.04})_{\Sigma 1}$ $Si_4O_{14}((OH)_{0.92}O_{0.87}F_{0.21})_{\Sigma 2}$ F_2,
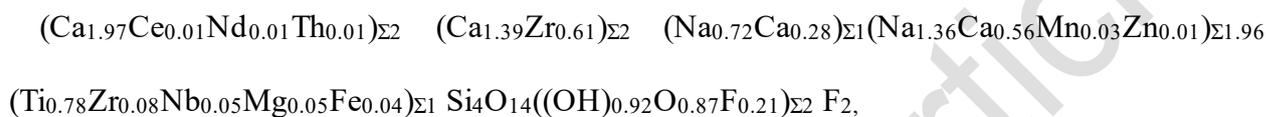
ideally $Ca_2(Ca_{1.5}Zr_{0.5})Na(NaCa)Ti(Si_2O_7)_2(O,OH)F_2$. The Lovozero bortolanite has the following differences from the holotype:

(1)   presence of (OH) groups and their predominance over F in X^O_M site. Thus, bortolanite from the Lovozero massif is essentially a separate (OH)-dominant mineral species; however, it is impossible to approve it in this status until enough material has been found for the quantitative determination of water;

(2)   some difference in electron density between the M^H and A^P positions compared to the same values for the Brazilian sample. It is associated with a higher content of Zr (M^H) and a lower content of *REE*s (A^P);

(3)   for some Lovozero samples, a certain deficiency in the sum of analyses persists after the charge balancing (Table 2). Some of the cations may be thought to be replaced by water molecules, which is typical of such cation-deficient species of the rinkite group as mosandrite-(Ce) and batievaite-(Ce).

There are still some discrepancies between the analytical data of chemical composition and structural model. The X^O_M position is tetrahedral, and in order to place (OH) groups instead of F in it according to the structural model vacancies in M^O3 are necessary. There are only 0.04 vacancies in M^O3 site, which is much less than the number of prospective (OH) groups – 0.92.

This problem seems to be unsolvable within this study. The development of research on rinkite group minerals, including minerals from the Lovozero massif, should help clarify the situation.

In the Lovozero massif, bortolanite, as well as other Ca-bearing rinkite group minerals, were found in two rock types. The first type is the contact of alkaline rocks with roof xenoliths (Figs 1 b,c, 2) or country rocks, and the second one is represented by poikilitic feldspathoid syenites (Figs 1 d,e, 3).

The main reason for such localization of bortolanite, rinkite-(Ce) and rosenbuschite is a low calcium content and a high Na/Ca ratio in the alkaline rocks of the Lovozero massif. According to Gerasimovsky and colleagues (1966), the average Na/Ca ratio in the nepheline syenites of the Lovozero massif is 9.39 while that in nepheline syenites elsewhere is 3.66. As a result, calcium minerals are rare in the alkaline rocks of the Lovozero massif (Semenov, 1972; Pekov, 2001), and calcium is incorporated in rock-forming sodium minerals (e.g., aegirine, magnesio-arfvedsonite, nepheline) as an impurity. Crystallization of calcium minerals in the Lovozero massif is possible (1) during metasomatism of calcium-enriched rocks or (2) in highly evolved rocks as a result of the accumulation of calcium in the melt. The roof xenoliths of the Lovozero massif are composed of basalt, basalt tuffs and tuffites and contain up to 15 wt.% CaO (Korchak et al. 2011). Under the influence of alkaline melts, a reaction rim composed of Na-Ca amphibole (ferri-katophorite), phlogopite, rosenbushite and bortolanite formed around the xenoliths.

Vlasov and colleagues (Vlasov et al., 1959) stated that poikilitic feldspathoid syenites represented a pegmatoid stage in the evolution of the Lovozero massif having been formed as a result of crystallization of a highly evolved melt enriched in volatile components and rare elements. Even though poikilitic rocks in the Lovozero massif are not widespread (5% of the massif volume), most of the rare metal pegmatites are confined to these rocks. Pegmatites that associate with poikilitic rocks are characterized by the greatest variety of lithium, beryllium and rare-earth minerals. Poikilitic feldspathoid syenites contain various calcium minerals, such as Na-Ca amphiboles, titanite and apatite supergroup minerals. It is likely that calcium gradually

accumulated as the earliest sodium-rich rocks of the massif crystallized, and it became possible for calcium minerals, including bortolanite, to crystallize in poikilitic feldspathoid syenites.

The chemical composition of bortolanite contains fingerprints of mineral-forming environment. Among the rocks of the massif, poikilitic syenites contain the highest concentrations of strontium and are enriched in potassium, and bortolanite from these rocks contains Sr and K impurities. Mg and Zn impurities in bortolanite from the reaction rims between xenoliths and alkaline rocks are apparently caused by the enrichment of volcanoclastic rocks with magnesian minerals.

It is noteworthy that there are *REE*s in bortolanite, but rosenbushite from the same rocks contain no rare earths (Table 2). Though, the Lovozero rosenbushite (Semenov, 1972) found in the "leucocratic nepheline syenite formed by changing the phonolite porphyry xenolith on the contact with apatite-titanite foyaite in association with amphibole, apatite, magnetite and lovenite" contains 2.05 wt.% *REE*s (this rosenbushite composition is plotted in Figure 3). Consequently, the *REE* content as such is not a characteristic feature of bortolanite, but in cases where both phases, bortolanite and rosenbushite, are formed as, for example, in the Lovozero rocks, the phase with a higher calcium content, i.e. bortolanite, becomes preferable for *REE*s.

The isomorphism of bortolanite with rosenbushite is clearly defined, especially with respect to the Lovozero samples. The Brazilian composition slightly deviates from the trend line due to the relatively low zirconium content (Fig. 3).

Competing interests

The authors declare none.

References

Agakhanov A. A., Day M. C., Sokolova E., Karpenko V. Yu., Hawthorne F. C., Pautov L. A., Pekov I. V., Kasatkin A. V., Agakhanova V. A. (2023) Two Rinkite-Group (Seidozerite-Supergroup) Minerals: Nacareniobsite-(Y), a New Mineral from the Darai-Pioz Alkaline Massif, Tajikistan, and Crystal-Structure Refinement of Nacareniobsite-(Ce). *The Canadian Journal of Mineralogy and Petrology,* 61, 1123-1136. doi:10.3749/2300029

Aksenov S.M., Ryanskaya A.D., Shchapova Yu.V., Chukanov N.V., Vladykin N.V., Votyakov S.L. and Rastsvetaeva R.K. (2021) Crystal chemistry of lamprophyllite-group minerals from the Murun alkaline complex (Russia) and pegmatites of Rocky Boy and Gordon Butte (USA): single crystal X-ray diffraction and Raman spectroscopy study. *Acta Crystallographica*, 77, 287–298.

Andrade M. B., Yang H., Downs R. T., Färber G., Filho R. R. C., Evans S. H., Loehn C.W. and Schumer B. N. (2018). Fluorlamprophyllite, $Na_3(SrNa)Ti_3(Si_2O_7)_2O_2F_2$, a new mineral from Poços de Caldas alkaline massif, Morro do Serrote, Minas Gerais, Brazil. *Mineralogical Magazine,* 82(1), 121-131.

Brese N.E. and O'Keeffe M. (1991) Bond-valence parameters for solids. *Acta Crystallographica*, 47, 192-197.

Brown I.D. and Altermatt D. (1985) Bond-valence parameters obtained from a systematic analysis of the inorganic structure database. *Acta Crystallographica*, 41, 244-247.

Bussen I. V. and Sakharov A. S. (1972) *Petrology of the Lovozero alkaline massif.* Nedra, Leningrad, 296 pp. (in Russian).

Chukanov N. V. and Vigasina M. F. (2020) Some Aspects of the Use of Raman Spectroscopy in Mineralogical Studies. In *Vibrational (Infrared and Raman) Spectra of Minerals and Related Compounds.* Springer International Publishing, 721-739.

CRYSALISPRO Software System, version 1.171.39.44. Rigaku Oxford Diffraction: Oxford, UK. 2015

Day M.C., Sokolova E., Hawthorne F.C., Horváth L. and Pfenninger-Horváth E. (2022) Bortolanite, $Ca_2(Ca_{1.5}Zr_{0.5})Na(NaCa)Ti(Si_2O_7)_2(FO)F_2$, a New Rinkite-Group (Seidozerite Supergroup) TS-Block Mineral from the Bortolan Quarry, Poços de Caldas Massif, Minas Gerais, Brazil. *The Canadian Mineralogist*, 60, 4, 699-712.

Dolomanov O.V., Bourhis L.J., Gildea R.J., Howard J.A.K. and Puschmann H. (2009) OLEX2: A complete structure solution, refinement and analysis program. *Journal of Applied Crystallography,* 42, 339–341.

Emsley J. (1980). Very strong hydrogen bonding. *Chemical Society Reviews*, 9(1), 91. doi:10.1039/cs9800900091

Ferraris G. (2008) Modular structures - the paradigmatic case of heterophyllosilicates. *Zeitschrift für Kristallographie – Crystalline Materials,* 223, 1-2, 76-84.

Ferraris G. and Gula A. (2005) Polysomatic Aspects of Microporous Minerals - Heterophyllosilicates, Palysepioles and Rhodesite-Related Structures. *Rev Mineral Geochem*. Vol. 57. P. 69-104.

Frezzotti M.L., Tecce F. and Casagli A. (2012) Raman spectroscopy for fluid inclusion analysis. *J. Geochemical Explor*. Vol. 112. P. 1–20.

Gerasimovsky V.I., Volkov V.P., Kogarko L.N., Polyakov A.I., Saprykina T.V. and Balashov Y.A. (1966) *Geochemistry of the Lovozero alkaline massif*. Nauka, Moscow, 396 pp. (in Russian).

Ilinca G. (2022) Charge Distribution and Bond Valence Sum Analysis of Sulfosalts – The ECoN21 Computer Program. *Minerals,* 12(8), 924.

Korchak Y.A., Men'shikov Y.P., Pakhomovsky Y.A., Yakovenchuk V.N. and Ivanyuk G.Y. (2011) Trap Formation of the Kola Peninsula. *Petrology,* 19, 1, 87-101. (In Russian).

Kramm U. and Kogarko L.N. (1994) Nd and Sr Isotope Signatures of the Khibina and Lovozero Agpaitic Centres, Kola Alkaline Province, Russia. *Lithos*, 32, 225–242.

Lafuente B., Downs R.T., Yang H. and Stone N. (2015) The power of databases: the RRUFF project. In: *Highlights in Mineralogical Crystallography,* Armbruster T. and Danisi R.M., eds. Berlin, Germany, De Gruyter W., pp 1-30.

Larkin P. J. (2011) *Infrared and Raman Spectroscopy: Principles and Spectral Interpretation*. Elsevier, 230 pp.

Libowitzky E. (1999).Correlation of O-H stretching frequencies and O-H···O hydrogen bond lengths in minerals. *Monatshefte Für Chemie / Chemical Monthly*, 130(8), 1047–1059. doi:10.1007/bf03354882

Lyalina L.M., Zolotarev A.A. Jr., Selivanova E.A., Savchenko Ye.E. , Krivovichev S.V., Mikhailova Yu.A., Kadyrova G.I. and Zozulya D.R. (2016) Batievaite-(Y), $Y_2Ca_2Ti[Si_2O_7]_2(OH)_2(H_2O)_4$, a new mineral from nepheline syenite pegmatite in the Sakharjok massif, Kola Peninsula, Russia. *Mineralogy and Petrology*,110(6), 895-904.

Mitchell R.H., Wu F.Y. and Yang Y.H. (2011) In Situ U-Pb, Sr and Nd Isotopic Analysis of Loparite by LA-(MC)-ICP-MS. *Chemical Geology*, 280, 191–199.

Pautov L.A., Agakhanov A.A., Karpenko V.Y., Uvarova Y.A., Sokolova E. and Hawthorne F.C. (2019) Rinkite-(Y), $Na_2Ca_4YTi(Si_2O_7)_2OF_3$, a seidozerite-supergroup TS-block mineral from the Darai-Pioz alkaline massif, Tien-Shan mountains, Tajikistan: Description and crystal structure. *Mineralogical Magazine*, 83: 373-380.

Pekov I.V. (2000) Lovozero Massif: History, Pegmatites, Minerals. Moscow: Ocean Pictures Ltd, 484 pp.

Saprykina L.G., Zhadritskii V.L., Panteleimonov V.M. and Tereshkov V.G. (1977) Report on Prospecting for Apatite within the Lovozero Alkaline Massif in 1974–76 and on the Search for

Apatite Ores in the Rocks of the Eudialyte Complex of the Northeastern Part of the Lovozero Massif in 1975–77 (Murmansk Region); Revda, Russia. (in Russian).

Semenov E.I. (1972) *Mineralogy of the Lovozero alkaline massif.* Nauka Publishing, Moscow, 308 pp. (in Russian).

Sharygin V.V., Stoppa F. and Kolesov B.A. (1996) Zr-Ti disilicates from the Pian di Celle volcano, Umbria, Italy. *European Journal of Mineralogy*, 8, 1199-1212.

Sheldrick G.M. (2015) Crystal structure refinement with SHELXL. *Acta Crystallographica*, 71, 3–8.

Sokolova E. (2006) From structure topology to chemical composition. I. Structural hierarchy and stereochemistry in titanium disilicate minerals. *The Canadian Mineralogist*, 44: 1273-1330.

Sokolova E. and Cámara, F. (2017) The seidozerite supergroup of TS-block minerals: nomenclature and classification, with change of the following names: rinkite to rinkite-(Ce), mosandrite to mosandrite-(Ce), hainite to hainite-(Y) and innelite-1T to innelite-1A. *Mineralogical Magazine*, 81(6), 1457-1484.

Vlasov K.A., Kuzmenko M.V. and Eskova E.M. (1966) *The Lovozero Alkali Massif.* Hafner Publishing, New York, 627 pp.

Wu F.Y., Yang Y.H., Marks M.A.W., Liu Z.C., Zhou Q., Ge W.C., Yang J.S., Zhao Z.F., Mitchell R.H. and Markl G. (2010) In Situ U-Pb, Sr, Nd and Hf Isotopic Analysis of Eudialyte by LA-(MC)-ICP-MS. *Chemical Geology*, 273, 8–34.